Journal of Materials Chemistry B

Accepted Manuscript

This article can be cited before page numbers have been issued, to do this please use: Y. Wang, B. Wang, H. Liao, X. Song, H. Wu, H. Wang, H. Shen, X. Ma and M. Tan, *J. Mater. Chem. B*, 2015, DOI: 10.1039/C5TB01197C.

ROYAL SOCIETY OF CHEMISTRY

www.rsc.org/materialsB

View Article Online
DOI: 10.1039/C5TB01197C

Journal of Materials Chemistry B

ARTICLE

Liposomal nanohybrid cerasomes for mitochondria-targeted drug delivery

Received 00th January 20xx,
Accepted 00th January 20xx

DOI: 10.1039/x0xx00000x

www.rsc.org/

Yanfang Wang,[ab] Beibei Wang,[ab] Han Liao,[ab] Xiaojie Song,[ab] Hao Wu,[ab] Huihui Wang,[ab] Hujun Shen,[d] Xiaojun Ma [a] and Mingqian Tan [ac*]

Mitochondrial dysfunctions cause numerous human disorders and the development of mitochondria-targted nanocarrier for drug delivery has aroused great attention. Herein, we report the synthesis of a liposomal nanohybrid cerasome modified with triphosphonium (TPP) for drug delivery to the mitochondrial matrix. The cerasomes were observed to possess an average size about 38 nm in diamater and the theoretical simulation of GBEMP mapping demonstrated the amphiphilic organotrialkoxysilanes was stable as a bilayer equilibrium conformation after self-assembly. The cerasomes showed good stability, excellent biocompatibility and sustainable drug release behavior. Moreover, the TPP-targeted cerasomes resulted in greater drug accumulation in mitochondria, thus leading to greater antitumor effect as compared to non-targeted cerasomes by using doxorubicin as a modal drug. The specific accumulation of TPP-targeted cerasomes within mitochondria was also confirmed by using JC-1 as fluorescent probe to analyze the mitochondrial transmembrane potential change.

Introduction

Mitochondrial dysfunction plays an important role in various human disorders, such as Alzheimer's disease (AD)[1], Parkinson's disease[2], diabetes[3], obesity[4, 5], and even cancer[6, 7]. There are already many kinds of drugs ranging from antioxidants for Alzheimer's disease[8] to chemotherapeutics for cancer and uncouplers of antioxidants phosphorylation for obesity[9, 10]. However, the key problem to develop the treatment of mitochondrial dysfunction disorders is how to delivery these drugs to the cell mitochondria safely and in sufficient amounts[11].

Among numerous drug delivery systems, liposomes attract particularly attention due to their good biocompatibility, capable of encapsulating hydrophilic drugs in the inner aqueous core and lipophilic drugs in the lipid bilayers[12, 13]. However, so far the liposome-based drug formulations have not widely used in clinic due to the poor stability, aggregation by proteins in blood[14]. In response to these limitations, liposomes based on Si-O-Si framework named the organic-inorganic hybrid cerasomes (CER) were recently introduced by Kiyofumi Katagiri[15]. Cerasomes are a kind of bio-inspired colloidal particles with a bilayer vesicular structure consisted of a polyorganosiloxane surface, which imparts cerasome much higher stability than conventional liposome. Cerasome was firstly used as drug delivery system for paclitaxel delivery, which exhibited controlled drug release and remarkably high stability, demonstrating that liposomal nanohybrid cerasomes can be a new promising drug delivery system[14]. Later on, doxorubicin (DOX)-loaded cerasomes were also reported to have the ability of controlled-drug release[16]. The sustained release of drugs from cerasomes can be modulated by alteration the vesicle composition[17].

In the development of theranostic drug delivery system to mitochondrial dysfunction, the most challenging problem is how to target the drug carriers to the mitochondria of the cells directly and to realize a sustained drug release. To solve this problem, a cation, called lipophilic triphenylphosphonium (TPP) cation, has been used to permeate the mitochondria membrane and accumulate in mitochondria matrix by changing mitochondria membrane potential[18-21]. TPP is able to permeate lipid bilayer easily and to accumulate several hundred fold within mitochondria because of its positive charge.[22] Therefore, introduction of mitochondria targeting moiety to the cerasomes is of great importance for the design and preparation of mitochondria-targeted nanocarriers for subcellular theranostics.

In this article, we developed an approach for the synthesis of TPP modified cerasome nanocarrier for mitochondrial targeted delivery of therapeutics. The cerasome-forming lipid (CFL) were synthesized through several steps. When dispersed

[a] Division of Biotechnology, Dalian Institute of Chemical Physics, Chinese Academy of Sciences, Dalian 116023, China. E-mail: mqtan@dicp.ac.cn; Fax: +86-411-82463027; Tel: +86-411-82463027
[b] University of the Chinese Academy of Sciences, Beijing 100049, China
[c] School of Food Science and Technology, Dalian Polytechnic University, Dalian 116034, China
[d] State Key Laboratory of Molecular Reaction Dynamics, Dalian Institute of Chemical Physics, Chinese Academy of Sciences, Dalian 116023, China.
† Electronic Supplementary Information (ESI) available: [details of any supplementary information available should be included here]. See DOI: 10.1039/x0xx00000x

† Yanfang Wang and Beibei Wang contributed equally to this work.

View Article Online
DOI: 10.1039/C5TB01197C

in acidic aqueous solution, CFL formed cerasomes via sol-gel self-assembly. Molecular dynamic simulation was considered as a complementary tool to experiment, which can provide an insightful understanding of the functions of biomaterials at a molecular and/or atomic level[23-25]. Herein, a coarse-grained (CG) modeling was employed for cerasome molecular dynamic simulation because the atomistic resolution of a biomolecular system can be properly reduced and the large-scale motions can be nicely preserved[26-30]. Gay-Berne (GB) potential[31-33], a well-known anisotropic potential, was also used for describing the van der Waals (VDW) interactions between the CG particles. The framework, by combining GB potential with point electric multipole (EMP) potentials[34-39], was adopted to model the silane bilayer system. Moreover, 3-aminopropyl triethoxysilane (APS) as a linker was conjugated with TPP (APS-TPP) to introduce TPP moiety on the surface of the cerasomes via the hydrolytic condensation of Si-OH between the nanoparticles and APS-TPP. The biocompatibility, time stability and structure stability of the resulted TPP-CER were investigated. Taken DOX as the model medicine and fluorochrome, TPP modified DOX-loaded cerasomes (TPP-CER-DOX) was studied for mitochondria-targeted drug delivery.

Experimental

Materials and Instruments

Hexadecylamine, bromohexadecane, dicyclohexylcarbodiimide (DCC), *N*-Hydroxysuccinimide (NHS), (3-aminopropyl)triethoxysilane (APS), 6-Bromohexanoic acid, triphenylphosphine, phosphotungstic acid and 3-(4,5-dimethylthiazol-2-yl)-2,5-diphenyltetrazolium bromide (MTT) were all purchased from Aladdin Reagents Co., Ltd. (Shanghai, China) and used without further treatment. Succinic anhydride was purchased from Institute of Guangfu Fine Chemical Engineering (Tianjin, China). The doxorubicin hydrochloride (DOX·HCl) was purchased from Meilun Biotech. Co. (Dalian, China). Curcumin (CUR) was purchased from Zelang Medical Technology Co., Ltd. (Nanjing, China). Mito-Tracker Deep Red FM was bought from Life Technologies Co., Ltd. (New York, USA). The solvents were all purchased from Beijing Chemical Works (Beijing, China) and all dried with molecular sieve before used. De-ionized water was prepared by a Mili-Q-Plus system (18.2 MΩ). Transmission electron microscopy (TEM) was performed using a JEOL JEM-2000EX Transmission electron microscope with a beam voltage of 120 kV in Dalian Medical University, China. The 200-230 mesh holey support films used for TEM were purchased from Zhongjingkeyi Technology Co., Ltd. (Beijing, China). The fluorescence images were acquired by laser scanning confocal microscope (LSCM). The amount of DOX and curcumin was measured by UV-visible spectrophotometer (UV 2550). Human cervical cancer Hela cell lines were purchased from Nanjing KeyGen Biotech. Co. Ltd. (Nanjing, China). JC-1(5, 59, 6, 69-tetrachloro-1, 19, 3, 39-tetra ethylbenzimidazol-carbocyanine iodide) (Beyotime Institute of Biotechnology, China). Syringe filter was purchased from Tianjing Jingteng Experiment Equipment Co., Ltd. (Tianjin China). Dynamic light scattering (Nano-ZS 90，Malvern, UK).

Cerasome preparation and characterization

CFL was synthesized as shown in Supporting Information (Scheme S1, Figure S1, S2 and S3, ESI). Cerasomes were prepared using a combined thin-film hydration and extrusion method according to the literature[40]. Briefly, chloroform solution containing N-[N-(3-Triethoxysilyl)propylsuccinamoyl] dihexadecylamine (compound 3, ESI) was evaporated out by a rotary evaporators to form a lipid film. The film was dried in a vacuum desiccator for 12 h to remove the residual methylene chloroform, and then hydrated in pH 3.0 HCl solution to form multi lamellar cerasome by vortexing for 15 min. The cerasomes were sonicated by a ultrasonic probe of 30W for 15 min to form vesicular membranes. The solution was placed at room temperature for 24 h to obtain Si-O-Si frame on the surface via the sol-gel processes. The size and size distribution of cerasomes were measured by transmission electron microscope (TEM) and dynamic light scattering (DLS).

Molecular dynamic simulation

The Gay-Berne electric multipole (GBEMP) parameters for the bond stretching, angle bending and torsional potentials were obtained by fitting to the atomistic profiles of the potentials of mean force (PMFs) constructed from atomic configurations (Optimized Potentials for Liquid Simulations, OPLS force field)[41] of liquid organics. All bonded parameters are given in Supporting Information. The GBEMP MD simulation protocol used in this study is described as follows. The atomistic structure of each system was converted into its CG representation in Euler coordinates containing three Cartesian coordinates (x, y and z) and three Euler angles (φ, ϑ and ψ) of the centers of mass. All GBEMP simulations were carried out in the generalized Kirkwood (GK) implicit solvent in the TINKER-based "GBEMP" program and the equation of motion was integrated using the Euler's rigid body integrator with an integration step of 10 fs[42]. The non-bonded interaction cutoff was set to 16 Å with a truncate scheme, and the Gay-Berne and electrostatic interactions of 1-2 and 1-3 neighbors were scaled with a factor of 0.003 and 1.0 respectively. Each nucleic acid system was minimized and subsequent runs were carried out under the temperature of 300 K for 20 ns.

Synthesis of CER-DOX and TPP-CER-DOX

The TPP-CER was synthesized by using APS as a linker to conjugate TPP and CER via the hydrolytic condensation of Si-OH of the cerasomes and siloxane of APS-TPP(Scheme S2, ESI). Detailed characterization of TPP-APS was given in Figure S4 and S5, ESI. Breifly, 1 mL APS-TPP in a syringe was pumped to 5 mL CER solution at a speed of 6.36 mL/h under stirring. The reaction was carried out at room temperature for 24 h to fully hydrolytic condensation. Sephadex G-50 chromatography was used to purify the TPP-CER and the filtrate was examined by UV-visible spectrophotometer and DLS.

As for drug encapsulation, a lipid film containing CFL was dried via rotary evaporator and vacuum desiccator, and then hydrated in the pH 3.0 HCl aqueous solution of DOX hydrochloride (0.575 mM). The modification of TPP on the

View Article Online
DOI: 10.1039/C5TB01197C

surface of CER-DOX was same as mentioned above. The resulted TPP-CER-DOX was dialyzed using a membrane with the cut-off limit 10 kDa in PBS. According to the literature[43], the fluorescence intensity of DOX encapsulated in liposomal structure was of 1/3 compare to that of equal concentration of free DOX. The concentration of DOX was determined by UV-visible spectrophotometer at 498 nm, while the loading of DOX was determined by fluorescent spectrophotometer at an excitation wavelength of 470 nm and the spectra was collected at the range of 515 to 800nm. For hydrophobic CUR encapsulation, the TPP-CER-CUR was prepared in a pH 3.0 HCl aqueous solution (containing 30 % (v/v) CH_3CH_2OH) of CUR (5.43mM) followed the same procedure of TPP-CER-DOX.

In Vitro Release

The hydrophilic DOX release from cerasomes in pH 7.4 phosphate buffer saline (PBS) was analyzed using a dialysis bag. Firstly, 5 mL of CER-DOX solution at a DOX encapsulated concentration of 0.293 mM was placed in a dialysis bag with a molecular weight cutoff of 10 kDa. Then the dialysis bag was immersed in a 100mL beaker containing 50 mL of pH 7.4 PBS. The beaker was incubated at 37 ^{o}C shaking tables. At the set time point, 2 mL of release medium was withdrawn from the beaker and another 2 mL fresh PBS was added to the beaker. The concentration of the DOX released from CER-DOX was measure by ultraviolet spectrophotometer. For hydrophobic curcumin, the dialysis medium was pH 3.0 HCl (containing 30% (v/v) CH_3CH_2OH) aqueous solution. To prevent biological contamination, 0.1% sodium azide was added to the dialysis medium.

Time Stability and Structure Stability

The time stability of CER was estimated by measuring the average size of CER solution using DLS. CER solution was hold at room temperature for 100 d. To determine the structure stability of CER, different volume of 50 mM Triton X-100 aqueous solution was added to 2 mL CER solution at room temperature and the average size of the solution was measured by DLS.

Drug Loading Capacity and Encapsulation Efficiency

The drug loading capacity (DLC) and encapsulation efficiency (EE) of drug-loaded CER were determined by microfiltration. Briefly, 5 mL of drug-loaded CER was placed in a syringe with a polyethersulfone filter, then the solution was pushed through the filter. The absorbance of the drug-loaded CER solution and filtrate was measured by ultraviolet spectrophotometer. Using the standard calibration curve, the amount of drug encapsulated in CER cerasomes was calculated.

The DLS and EE were evaluated by the following formulas[17, 44, 45].

$$DLC = \frac{\text{The amount of drug encapsulated in CER}}{\text{The total amount of CER}} \times 100\%$$

$$EE = \frac{\text{The amount of drug encapsulated in CER}}{\text{The initial amount of drug}} \times 100\%$$

Cytotoxicity Evaluation

In vitro cytotoxicity of CER and TPP-CER was evaluated by a MTT assay. The CER and TPP-CER were diluted with RPMI-1640 medium (containing 10% fetal bovine serum) to different concentrations, respectively. L929 cells were inoculated into 96-wells plates at a density of 5×10^3 cells per well in 200 μL of RPMI-1640 medium (containing 10% FBS) and incubated at 37 ^{o}C in CO_2 incubator for 48 h. Then the medium was replaced with 200 μL of CER and TPP-CER solutions aforementioned and the cells were incubated for an additional 24 and 48 h. The medium was replaced with 200 μL of culture medium containing 0.5 mg/mL MTT and the plates were incubated for 4 h. After that, the medium was removed and 200 μL of DMSO was added to each well to dissolve the formazan crystal. The dissolved solutions were transferred to another 96-well plate, and the optical density (OD) of the cells was measured by a microplate reader (Wellscan MK 3, Labsystem Dragon, USA) at 570 nm by using 630 nm as a reference. Cell viability was calculated through comparison with the control, which was the cells without any treatment by the CER.

Anti-tumor experiments

In vitro biological efficacy of CER-DOX and TPP-CER-DOX was also evaluated by the MTT assay. These cerasomes were diluted with RPMI-1640 medium (containing 10% FBS) to different DOX concentrations and free DOX solutions at the same concentration were used as control. We chose two types of cells: Hela cells and NCI cells, which were inoculated into 96-wells plates at a density of 5×10^3 cells per well in 200 μL of RPMI-1640 medium (containing 10% fetal bovine serum) and incubated at 37 ^{o}C in CO_2 incubator for 48 h. Then the cell medium was replaced with 200 μL of the DOX、CER-DOX and TPP-CER-DOX solutions aforementioned and the cells were incubated for an additional 24 and 48 h. The medium was replaced with 200 μL culture medium containing 0.5 mg/mL MTT and the plates were incubated for 4 h. After that, the medium was removed and 200 μL DMSO was added to each well to dissolve the formazan crystal. The dissolved solutions were transferred to another 96-well plate, and the cell OD values were measured by a microplate reader (Wellscan MK 3, Labsystem Dragon, USA) at 570 nm by using 630 nm as a reference. Cell viability was calculated through comparison with the control cells without any treatment by the CER.

Quantification of TPP-CER in Subcellular Compartments

Hela cells were inoculated into 35-mm dishes at a density of 5×10^5 cells per dish in 1 mL of RPMI-1640 medium (containing 10% fetal bovine serum) and incubated at 37 ^{o}C in CO_2 incubator for 24 h. The cells were treated with TPP-CER-DOX or CER-DOX for 3.5 h, then Mito-Tracker Deep Red FM was added to the medium and the cells were incubated for another 0.5 h. After the treatment, the cells were washed thrice with pH 7.4 PBS. The quantification of TPP-CER in subcellular compartments was then acquired by LSCM. Oil inserted 60x and 100x objective lens were used in xy and xyz mode with 800×800 pixel resolution. DOX was excited with a 488 nm line and emission was collected between 520-600 nm, while Mito-Tracker Deep Red FM was excited with a 633 nm laser and emission was collected between 666-698 nm.

Isolation of Mitochondria from cytosolic Extracts

View Article Online
DOI: 10.1039/C5TB01197C

Quantification of TPP-CER in subcellular compartments was further carried out by isolating mitochondria from cytosolic extracts through differential centrifugation. Briefly, Hela cells were inoculated into 90-mm dishes at a density of 2×10^6 cells per dish in 5 mL of RPMI-1640 medium (containing 10% fetal bovine serum) and incubated at 37 °C in CO_2 incubator for 48 h. The cells were treated with TPP-CER-DOX or CER-DOX for 4 h, and then the cells were washed thrice with pH 7.4 PBS. The cells were collected and put into a glass homogenizer for homogenizing. Until more than 50% cells were broken, the solution was centrifuged at 1000G for 10 min to precipitate the cell debris, and then the supernatant was centrifuged at 15 000 G for 10 min to isolate mitochondria from cytosolic extracts. Mitochondria were quantified with cytosolic extracts at the wavelength of 488 nm by UV-visible spectrophotometer (UV 2550).

Detection of the mitochondrial transmembrane potential

Mitochondrial transmembrane potential was evaluated by a mitochondrial membrane potential assay kit with JC-1. Hela cells were inoculated into 35-mm dishes at a density of 5×10^5 cells per dish in 1 mL RPMI-1640 medium (containing 10% fetal bovine serum) and incubated at 37 °C in CO_2 incubator for 24 h. The cells were treated with or without of TPP-CER-DOX or CER-DOX for 4 h. After the treatment, the cells were incubated in JC-1 solution (5 μg/mL) for another 0.5 h. The cells were washed thrice with pH 7.4 PBS and quantified by laser LSCM. Oil inserted 60x and 100x objective lens were used in xy and xyz mode with 800×800 pixel resolution. J-aggregates (J-Aggr) were excited with a 543 nm laser and emission was collected between 550-650 nm, while J-monomer was excited with a 488 nm laser and emission was collected between 500-540 nm.

Results and discussion

The use of both TPP and cerasomes has tremendous potential to make an effective mitochondria-targeted nanocarrier due to several advantages. Firstly, the cerasomes have much higher stability than conventional liposome, which exhibited controlled drug release property. Secondly, the surface of the cerasomes can also be modified to provide further functionality, such as targeting agents, or fluorescent agents, to make targeted or multimodal imaging agents, respectively. Thirdly, as a targeting agent, the TPP with positive charge is able to easily permeate lipid bilayers and to accumulate within the mitochondria because of the large membrane potential (-150 to -70 mV, negative inside), resulting in highly efficient mitochondrial uptake.[22] Herein, the formation of TPP-targeted drug-loaded cerasomes (TPP-CER-DOX) is illustrated in Fig. 1. Taken DOX as the model drug and fluorescent agent, DOX-loaded cerasomes (CER-DOX) were prepared through a combined film hydration and self-assembly process. Mitochondria-targeted molecules TPP was conjugated to CER-DOX by using APS and 6-bromohexanoic acid as linkers. The TPP-CER-DOX can permeate lipid bilayers and enter the cells by clathrin-mediated endocytosis[43]. This results in the mitochondria targeting and the encapsulated drug release to realize the therapy and imaging of mitochondrial at a subcellular level.

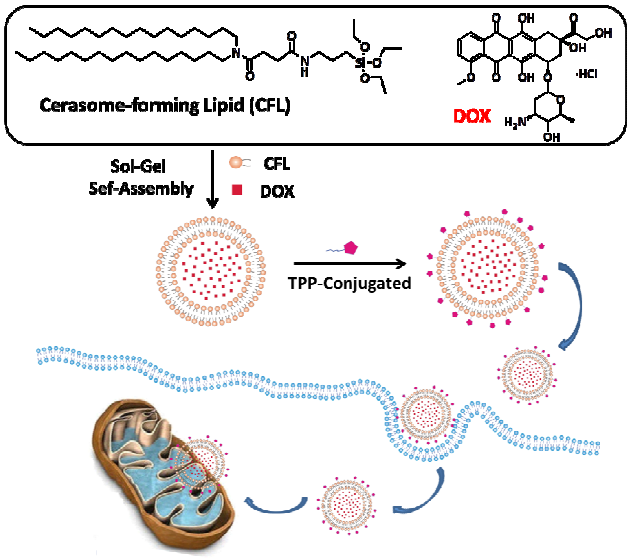

Fig.1: Schematic illustration of the formation process of the Doxorubicin-loaded cerasomes (CER-DOX) and TPP modified cerasomes (TPP-CER-DOX). CFL: cerasome-forming lipid.

Synthesis of cerasomes

The detailed synthesis of CFL was described in the electronic supplementary information (ESI). The resulted CFL was then hydrated in the pH 3.0 HCl aqueous solution in the absence or presence of DOX hydrochloride to form cerasomes or CER-DOX, respectively, through the self-assembly approach. The TEM image of the obtained cerasomes in Fig. 2A revealed that they owned spherical morphology with an average size about 38 nm and a narrow size distribution (Fig. 2B), while the hydrodynamic diameter of cerasomes measured by DLS was about 210 nm. As we know, by TEM we image single particle, while DLS gives an average size estimation, which is biased toward the larger-size end of the population distribution because large particles scatter the light much more intensely than smaller particles. These results were also reported in previous literature.[46]

The TPP-CER nanoparticles were prepared by surface modification of CER with TPP-APS. The characteristic absorption peak of TPP-COOH was at 262, 268 and 274 nm (Fig. 2C). After the purification of Sephadex G-50 chromatography, the TPP-CER not only shows the TPP absorbance as illustrated in Fig.2 C, but also can be detected with DLS (Fig.2 D), while the small molecule TPP only has the absorption peak and can not be detected by DLS. The results further demonstrated that TPP-CER nanoparticles were successfully prepared. The number of TPP molecules per cerasome was calculated to be 415. The DLS data showed that the average size of CER-DOX and TPP-CER-DOX nanoparticles was about 226 and 220 nm (Fig. S6), respectively. The CER-DOX and TPP-CER-DOX had a very close size and size distribution. The encapsulation of DOX and the modification of TPP on the surface of cerasome didn't

View Article Online
DOI: 10.1039/C5TB01197C
Journal of Materials Chemistry B ARTICLE

affect their hydrophilcity. The Zeta potential of the CER, TPP-CER and CER-DOX was shown in Table S1.The zeta-potential of CER and TPP-CER in neutral condition is –18.61±6.41 mV and +15.37±0.68 mV, respectively. As for CER-DOX, the zeta-potential is –13.49±2.17 mV and the loaded DOX didn't change the surface charge of CER significantly, which is consistent with the previous report.[16]

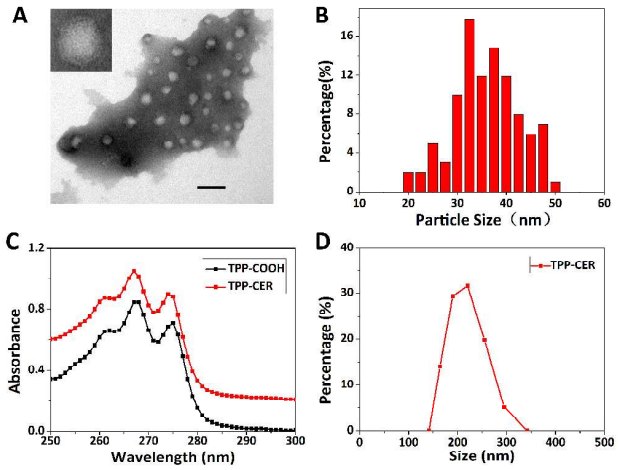

Fig. 2: (A)TEM image of cerasomes, inset shows the enlarged TEM image of single cerasome; inset shows the enlarged single particle. Scale bar= 100 nm. (B) Size distribution of cerasomes measured by TEM. (C) The characteristic absorption peak of TPP-COOH and TPP-CER. (D) DLS size distribution of the filtrate containing TPP-CER that has the same characteristic absorption peak with TPP-COOH, while that containing small molecule TPP-COOH was not detected by the DLS.

Molecular dynamic simulation was adopted herein as a complementary tool to further understand the formation of cerasomes at a molecular and/or atomic level. We constructed a starting structure containing 72 CFL molecules to simulate the formation of cerasomes (Fig. 3A and 3B). Gay-Berne electric multipole (GBEMP) mapping for silane is depicted in Fig. S8. The CG model is composed of three elliptic rigid bodies and one spherical rigid body. The hydrophobic tail of the silane model is represented by two elliptic rigid bodies in each of which contains one Gay-Berne site and one non-interacting EMP site. The non-interacting EMP site (denoted by orange filled circle) would not involve in electrostatic interaction but serve just as the connection purpose. As for the hydrophilic head group, the elliptic rigid body contains one Gay-Berne site and two EMP interacting sites while the spherical rigid body contains one Gay-Berne site and one EMP site which both share a same location shown by a red filled circle. GBEMP energy function can be seen in the ESI. To parametrize the Gay-Berne potentials for the CG models (Fig. S8), the atomistic energy profiles (using OPLS atomistic force field) were constructed for the intermolecular van der Waals (VDW) interactions between two identical molecular fragments (homodimer), illustrated in Fig. S9. In each case, diverse configurations were generated with different orientations (such as, cross, end-to-end, face-to-face, etc.) as well as at various separations. The initial Gay-Berne parameters for CG particles were derived through fitting to the corresponding atomistic energy profiles in gas phase using a genetic algorithm. The potential energies have been monitored during the GBEMP simulation. For the system, the energy landscape became flat after 10 ns simulation, indicating the systems reach its equilibrium. From Fig. 3 C, one can see that the bilayer structure is supposed to be stable as an equilibrium conformation. The structural properties of the final equilibrium conformation are given in Table 1. The thickness of the membrane of CER measured from the TEM images was 5.81±0.96 nm (Fig. 2 A, inset), which is close to the thickness obtained from GMEMP simulation.

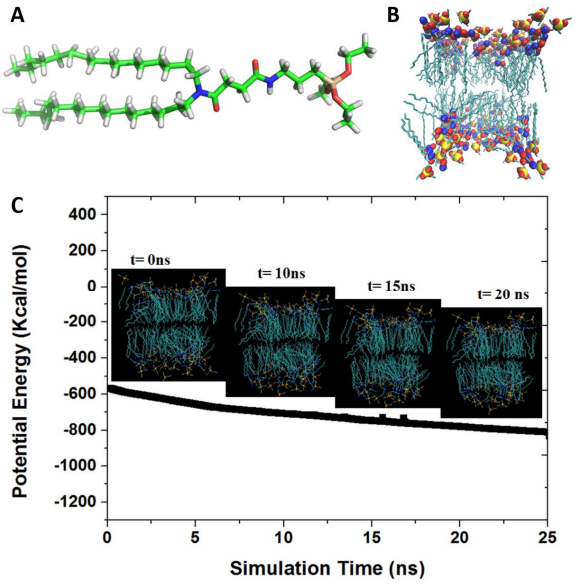

Fig. 3: (A) CFL structure model. (B) The bilayer structure of cerasomes system. (C) Potential energies of the system evolving with MD simulation time. The starting structure (t = 0 ns) of the system was constructed as a form of bilayer.

Table 1. Structural parameters of the 72 silane bilayer system, obtained from GBEMP simulation.

Structural Parameters	GBEMP Model
Thickness D_{HH} (Å)	53.0
Area per lipid A_L (Å^2)	68.5
Volume per lipid V_L (Å^3)	1825.0

In vitro drug release and cytotoxicity

Like liposome, cerasome is composed with an internal aqueous compartment and a hydrophobic interval of the bilayer membrane. The internal aqueous compartment can encapsulate hydrophilic drugs, while the hydrophobic interval of the bilayer membrane can carry hydrophobic drugs. Taken DOX and CUR as the models of hydrophilic and hydrophobic drugs, respectively, drug-loaded cerasomes were prepared and purified. The encapsulation efficiency (EE) was evaluated to be 3.34 % and 33.29 % and the drug loading capacity (DLC) was 53.40 % and 92.15 %, respectively. Fig. 4A shows the accumulative DOX and CUR release profile. Dialysis bags

View Article Online
DOI: 10.1039/C5TB01197C

containing CER-DOX and CER-CUR were placed in PBS and PBS/CH_3CH_2OH solutions, respectively, while both CER-DOX and CER-CUR had a sustained release within 24 h at 37 °C. As shown in Fig. 4A, 36.85 % and 46.02 % of the encapsulated DOX and CUR released from cerasomes within 24 h, indicating a remarkable controlled-release of both hydrophilic and hydrophobic drugs.

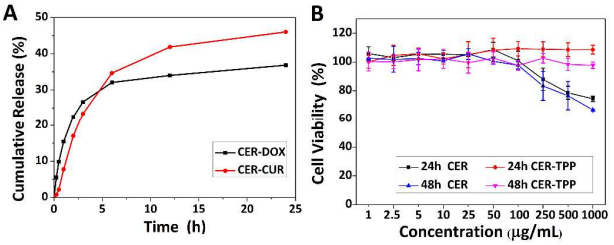

Fig. 4: (A) Release of DOX from CER-DOX and Curcumin from CER-CUR in 24 h. (B) In vitro cytotoxicity of cerasomes (CER) and TPP-modified cerasomes (TPP-CER) (n=3) at 24 h and 48 h, respectively, for L929 cells.

To verify the biocompatibility of TPP-CER, the cytotoxic effects of CER and TPP-CER were evaluated in L929 cells by MTT assays. As shown in Fig. 4B, cell viability remained around 100 % for both CER and TPP-CER after 24 h or 48 h incubation at the concentration less than 100 μg/mL. When the concentration was more than 100 μg/mL, the cell viability of TPP-CER was still around 100%, while that of CER was gradually reduced with the increase of the concentration and the incubation time. When L929 cells were incubated with CER of 1000 μg/mL for 24 h and 48 h, the cell viability was decreased to 74% and 67%, respectively. Previous works demonstrated that CER had lower cytotoxicity than silica nanoparticles,[47] but mild cytotoxicity than liposomes[17]. In this case, the CER showed growth inhibition in a concentration- and time-dependent manner in L929 cells from 1 to 1000 μg/mL, and the modification of TPP enhanced the biocompatibility of CER.

In Vitro Anti-tumor effect

NCI and Hela cells were chosen to evaluate the *in vitro* anticancer performance of free DOX、CER-DOX and TPP-CER-DOX with equal concentration of DOX. Fig. 5 shows the results of cell viability measured by MTT assay for 24 and 48 h, respectively. As for the Hela cells incubated for 24 h, when the concentration of DOX was below 100 nM, the cell viability of free DOX was above 90%, while the cell viability decreased to 27.67% with the increase of DOX concentration (Fig. 5A). The cell viability of CER-DOX and TPP-CER-DOX was higher than that of free DOX. For CER-DOX, the cell viability maintained around 100% with concentration change. The cell viability of TPP-CER-DOX was somewhat lower than that of CER-DOX. From 1 to 500 nM, the cell viability was more than 90%, while the cell viability decreased to 82% at the concentration of 2500 nM. When the incubating time increased to 48 h, the cell viability of free DOX decreased to 18% with the increase of DOX concentration from 50 to 2500 nM (Fig. 5B). The cell viability of CER-DOX and TPP-CER-DOX was also higher than that of free DOX, and the cell viability of TPP-CER-DOX was somewhat lower than CER-DOX. The cell viability of CER-DOX and TPP-CER-DOX decreased to 82% and 77% with the increase of DOX concentration. The result indicated that the cell viability decreased with the increase of incubating time. As for NCI cells, the cell viability of free DOX decreased to 45% and 14% with the increase of DOX concentration from 50 to 2500 nM at 24 h and 48 h, respectively (Fig. 5C and 5D). The tendency of cell viability of CER-DOX and TPP-CER-DOX incubating with NCI cells was similar to that of Hela cells. The cell viability of CER-DOX and TPP-CER-DOX was also higher than that of free DOX. Moreover, the cell viability of CER-DOX and TPP-CER-DOX decreased with the increase of DOX concentration. The concentration of free DOX was equal to that of DOX encapsulated in the cerasomes, while the cell viability of encapsulated DOX was lower than that of free DOX, due to the shielding effects of the cerasomes. It should be pointed out that the TPP-CER-DOX resulted greater cytotoxicity than CER-DOX probably because it targeted the mitochondria of the cells and led to stronger cytotoxicity. However, the efficacy of the TPP-CER-DOX does not look so great even at 48 h due to the sustained release of DOX from the nanocarriers. Although more than 30% DOX can be released from CER-DOX in 24 h (Figure 4A), the results revealed that released DOX can not kill the cells so effectively as those free DOX. Similar result was also reported in previous work of monodisperse hollow mesoporous silica (HMS) nanocages as nanocages for drug delivery[48]. Further animal treatment study will be conducted to evaluate the potential of the nanodrug

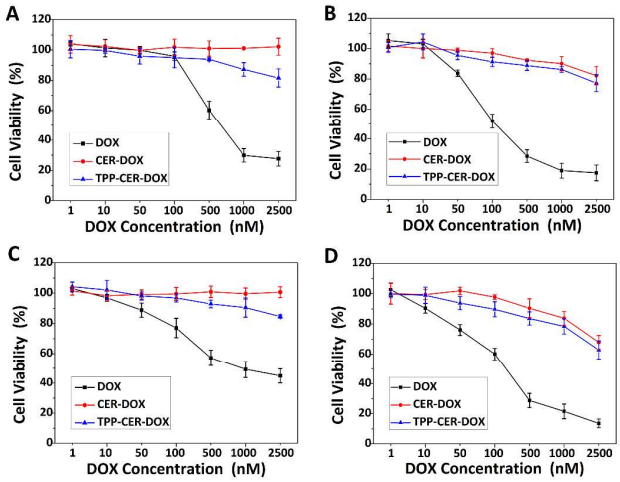

Fig. 5: Cytotoxicity of free DOX, CER-DOX and TPP-CER-DOX for Hela cells and NCI cells incubated for 24 and 48h, respectively. (A) 24h, Hela cells; (B) 48h, Hela cells; (C) 24h, NCI cells; (D) 48h, NCI cells.

In vitro Mitochondrial Targeting effect

In order to assess the effectiveness of TPP-conjugated cerasomes for mitochondria localization in cells, the co-localization of TPP-CER-DOX was investigated in human cervical cancer Hela cells by using a mitochondria-tracker (Deep Red) as reference. Hela cells were incubated with the CER-DOX and TPP-CER-DOX for 4 h in serum medium, followed by washing with PBS and stained with mitochondria-tracker for

View Article Online
DOI: 10.1039/C5TB01197C

30 min. Fluorescence micrographs of red and green stand for the distribution of cerasomes and mitochondria-tracker, respectively. They were overlaid and co-located in yellow by LSCM. Fig. 6 shows the distribution of the non-targeted CER-DOX and the targeted TPP-CER-DOX in Hela cells. Some of CER-DOX signals were from mitochondrial, but there is no signal from nuclei (Fig. 6A). Previous work suggested that the cellular uptake of cerasomes occurred probably through a process of clathrin-mediated endocytosis, which resulted in rearrangement of the cell cytoskeleton.[47] Since the CER-DOX and TPP-CER-DOX particles were incubated with Hela cell for only 4 h, the amount of released DOX targeted in the nuclei was not sufficient and no fluorescence signal was seen from nuclei area. Moreover, there existed significant co-localization of the TPP-CER-DOX with mitochondria-tracker in the mitochondria of cells, while the red signals of non-targeted CER-DOX and mitochondria-tracker differed in position. Quantitative analysis of the fluorescence images in each group, the Pearson's coefficient of targeted TPP-CER-DOX was 0.760 ± 0.037, while that of non-targeted CER-DOX was only 0.535 ± 0.135. The Pearson's coefficient increased averagely by 22.5%. The results demonstrated that the TPP modified cerasomes TPP-CER-DOX could promote the cerasomes entering mitochondria to release drug in the mitochondria. Such efficient mitochondria-targeted drug delivery by the cerasome system is promising for long-term mitochondria-targeted therapy.

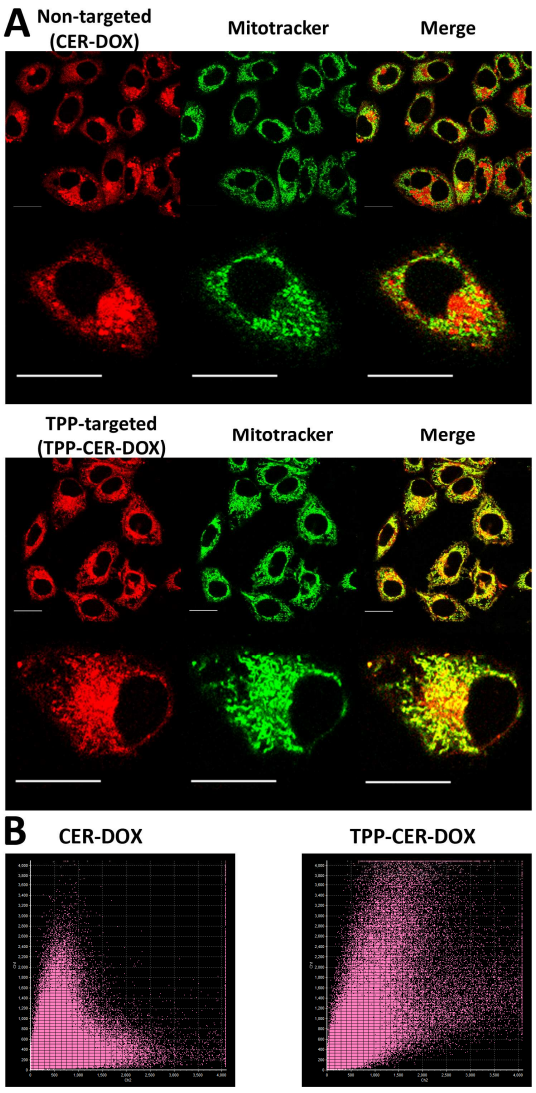

Fig. 6: Mitochondrial localization of CER-DOX and TPP-CER-DOX. Hela cells were exposed to non-targeted CER-DOX and TPP-targeted TPP-CER-DOX for 4 h (Scale bar: 20 μm). The cells were then stained with mitochondrial marker Mito-Tracker Deep Red for 30 min. The staining solution was washed by pH 7.4 PBS and the cells were observed by fluorescence microscopy. (A)The merge images showed that the overlap of Mito-Tracker (Green) and CER-DOX (Red) was unobvious (Top), while the overlap of TPP-CER-DOX was significant (Down). (B) The Pearson's Coefficient analysis plots of CER-DOX (left) and TPP-CER-DOX (right).

Analysis of Mitochondrial Transmembrane Potential

The mitochondrial membrane potential could be reduced due to the increasing of proton permeability of the mitochondrial inner membrane caused by the accumulation of lipophilic cations, such as TPP, within the mitochondria [49]. Therefore, to further confirm the TPP-CER-DOX accumulation within mitochondria, the mitochondrial transmembrane potential was analyzed in Hela cells. Herein, the fluorescent probe JC-1 was used for detection of mitochondrial membrane potential. It is well know that when the membrane potential is high, JC-1 aggregates in mitochondrial matrix to emit red light. When the

View Article Online
DOI: 10.1039/C5TB01197C

membrane potential is low, JC-1 presents in cytoplasm in the form of monomers to emit green light. The proportion of red/green fluorescence intensity can represent the change of mitochondrial membrane potential. The red fluorescence of CER-DOX in Fig. 7A is stronger than that of TPP-CER-DOX, while the green fluorescence is weaker than that of TPP-CER-DOX, suggesting that the mitochondrial membrane potential became smaller for the case of TPP-CER-DOX and the JC-1 was more easily presented in cytoplasm in the form of monomers to emit green light. The quantification of the red/green fluorescence intensity proportion for CER-DOX was 0.620, while it was only 0.476 for TPP-CER-DOX, which means the proportion of red/green fluorescence intensity of CER-DOX is greater than that of TPP-CER-DOX(Fig. 7B). Compared to CER-DOX, the results demonstrated that the mitochondrial membrane potential decreased, indicating better accumulation ability of TPP-CER-DOX within the mitochondria.

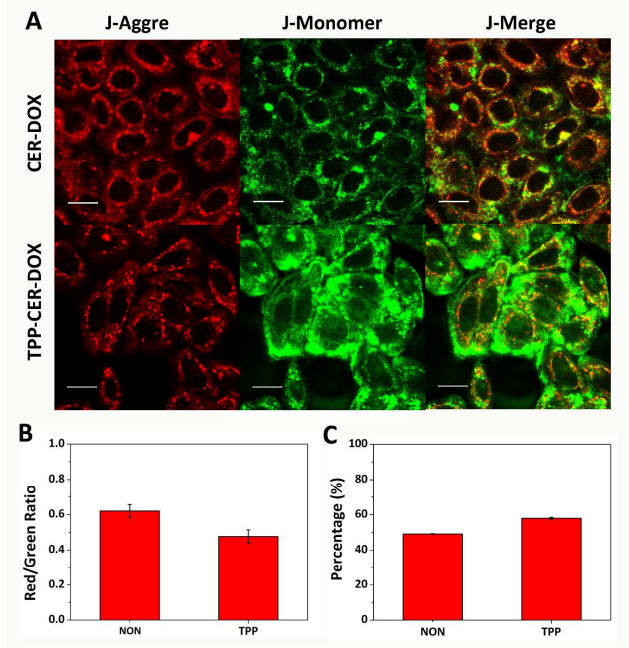

Fig. 7: (A) Fluorescence images of Hela cells incubated with CER-DOX or TPP-CER-DOX by using fluorescent probe JC-1 to indicate the mitochondrial transmembrane potential change (Scale bar: 40 μm). When the membrane potential is high, JC-1 aggregated in mitochondrial matrix as JC-1 aggregates to emit red light (585/590 nm). When the membrane potential is low, JC-1 presented in cytoplasm in the form of monomers to emit green light (514/529 nm). The proportion of red and green fluorescence intensity can represent the change of mitochondrial membrane potential. (B) The proportion of red and green fluorescence intensity of Hela cells incubated with CER-DOX and TPP-CER-DOX for 4 h. (C) The proportion of mitochondria extracts in Hela cells incubated with CER-DOX and TPP-CER-DOX for 4 h, respectively.

In addition, to further quantify the accumulation of TPP-CER-DOX in mitochondria, the mitochondria were isolated from and cytosolic extracts through differential centrifugation. The CER-DOX and TPP-CER-DOX accumulated in different part of the cells after incubation. Differential centrifugation made the cytoplasm and mitochondria precipitated at the specific centrifugal speed. The absorbance of DOX in mitochondria and cytoplasm at the wavelength of 488 nm was analyzed by UV-visible spectrophotometry to determine the accumulated DOX amount. The results showed that the proportion of CER-DOX accumulated in mitochondria was 51.87%, while that of TPP-CER-DOX was 60.16% (Fig. 7C). Compared to CER-DOX, the proportion of TPP-CER-DOX accumulated in mitochondria increased about 8.29 %, further suggesting the specific accumulation ability of the TPP-CER-DOX in mitochondria-targeted drug delivery.

Conclusions

In summary, we have developed a general and facile synthesis method to fabricate TPP modified liposomal cerasome that could be applied as nanocarrier for mitochondria-targeted therapeutics by using DOX as model medicine. The cerasomes were prepared via the self-assembly and sol-gel reaction of amphiphilic organotrialkoxysilanes to form bilayer vesicles covered with a silicate surface. The APS-TPP targeting moiety was conjugated on the cerasomes to specifically recognize the mitochondria. The stability of cerasome was good due to the siloxane network formed on the cerasome surface. The theoretical simulation of GBEMP mapping demonstrated the amphiphilic organotrialkoxysilanes was supposed to be stable as a bilayer equilibrium conformation after self-assembly. The cerasomes showed excellent biocompatibility and had a sustained release ability within 24 h at 37 ^{o}C after loading the drugs of DOX or CUR. Taken DOX as the model medicine and fluorochrome, the TPP-CER-DOX resulted in greater drug accumulation in mitochondria as compared to non-targeted CER-DOX. The quantitative analysis of mitochondrial transmembrane potential further confirmed the remarkable accumulation ability of TPP-CER-DOX within the mitochondria. We believe that the TPP modified cerasome may have potential as nanocarrier for mitochondria-targeted theranostics.

Acknowledgements

This work was supported by the National Nature Science Foundation of China (91227126), National Special Fund for Key Scientific Instrument and Equipment Development (2013YQ17046307) and the Nature Science Foundation of Liaoning Province, China (2013020177).

References

1. A. Nunomura, G. Perry, G. Aliev, K. Hirai, A. Takeda, E. K. Balraj, P. K. Jones, H. Ghanbari, T. Wataya and S. Shimohama, *J. Neuropathol. Exp. Neurol.*, 2001, **60**, 759-767.
2. S. Kösel, G. Hofhaus, A. Maassen, P. Vieregge and M. B. Graeber, *Biol. Chem.*, 1999, **380**, 865-870.
3. B. B. Lowell and G. I. Shulman, *Science*, 2005, **307**, 384-387.
4. J. Martinez, *J. Physiol. Biochem.*, 2006, **62**, 303-306.
5. F. I. Milagro, J. Campión and J. A. Martínez, *Obesity*, 2006, **14**, 1118-1123.
6. M. R. Duchen, *Mol. Aspects Med.*, 2004, **25**, 365-451.

View Article Online
DOI: 10.1039/C5TB01197C

7. L. Galluzzi, E. Morselli, O. Kepp, I. Vitale, A. Rigoni, E. Vacchelli, M. Michaud, H. Zischka, M. Castedo and G. Kroemer, *Mol. Aspects Med.*, 2010, **31**, 1-20.
8. K. Ono, K. Hasegawa, H. Naiki and M. Yamada, *J. Neurosci. Res.*, 2004, **75**, 742-750.
9. A. Floridi, M. G. Paggi, M. L. Marcante, B. Silvestrini, A. Caputo and C. de Martino, *J. Natl. Cancer Inst.*, 1981, **66**, 497-499.
10. J. Harper, K. Dickinson and M. Brand, *Obes. Rev.*, 2001, **2**, 255-265.
11. S. Fulda, L. Galluzzi and G. Kroemer, *Nat. Rev. Drug Discov.*, 2010, **9**, 447-464.
12. A. Jesorka and O. Orwar, *Annu. Rev. Anal. Chem. (Palo Alto Calif)*, 2008, **1**, 801-832.
13. L. Zhang, J. M. Chan, F. X. Gu, J.-W. Rhee, A. Z. Wang, A. F. Radovic-Moreno, F. Alexis, R. Langer and O. C. Farokhzad, *ACS nano*, 2008, **2**, 1696-1702.
14. Z. Cao, Y. Ma, X. Yue, S. Li, Z. Dai and J. Kikuchi, *Chem. Commun.*, 2010, **46**, 5265-5267.
15. K. Katagiri, K. Ariga and J.-i. Kikuchi, *Chemistry Letters*, 1999, 661-662.
16. Y. Jin, X. Yue, Q. Zhang, X. Wu, Z. Cao and Z. Dai, *Acta Biomater.*, 2012, **8**, 3372-3380.
17. Z. Cao, X. Yue, Y. Jin, X. Wu and Z. Dai, *Colloids Surf., B*, 2012, **98**, 97-104.
18. L. B. Chen, *Annu. Rev. Cell Dev. Biol.*, 1988, **4**, 155-181.
19. R. A. Smith, C. M. Porteous, A. M. Gane and M. P. Murphy, *Proc Natl Acad Sci USA*, 2003, **100**, 5407-5412.
20. L. Grinius, A. Jasaitis, Y. P. Kadziauskas, E. Liberman, V. Skulachev, V. Topali, L. Tsofina and M. Vladimirova, *BBA-Bioenergetics*, 1970, **216**, 1-12.
21. M. P. Murphy and R. A. Smith, *Adv. Drug Deliv. Rev.*, 2000, **41**, 235-250.
22. R. A. Smith, C. M. Porteous, A. M. Gane and M. P. Murphy, *Proc Natl Acad Sci U S A*, 2003, **100**, 5407-5412.
23. M. Karplus and J. A. McCammon, *Nat. Struct. Mol. Biol.*, 2002, **9**, 646-652.
24. M. Karplus and J. Kuriyan, *PNAS*, 2005, **102**, 6679-6685.
25. A. Pérez, F. J. Luque and M. Orozco, *Acc. Chem. Res.*, 2011, **45**, 196-205.
26. P. Sherwood, B. R. Brooks and M. S. Sansom, *Curr. Opin. Struct. Biol.*, 2008, **18**, 630-640.
27. V. Tozzini, *Curr. Opin. Struct. Biol.*, 2005, **15**, 144-150.
28. V. Tozzini, *Acc. Chem. Res.*, 2009, **43**, 220-230.
29. H. Shen, Z. Xia, G. Li and P. Ren, *Annu. Rep. Comput. Chem.*, 2012, **8**, 129-148.
30. B. A. Merchant and J. D. Madura, *Annu. Rep. Comput. Chem.*, 2011, **7**, 67-87.
31. D. J. Cleaver, C. M. Care, M. P. Allen and M. P. Neal, *Phys Rev E*, 1996, **54**, 559.
32. B. J. Berne and P. Pechukas, *J. Chem. Phys.*, 1972, **56**, 4213-4216.
33. J. Gay and B. Berne, *J. Chem. Phys.*, 1981, **74**, 3316-3319.
34. P. A. Golubkov and P. Ren, *J. Chem. Phys.*, 2006, **125**, 064103.
35. P. A. Golubkov, J. C. Wu and P. Ren, *Phys. Chem. Chem. Phys.*, 2008, **10**, 2050-2057.
36. P.-J. XU, Y.-Y. TANG, J. ZHANG, Z.-B. ZHANG, K. WANG, Y. SHAO, H.-J. SHEN and Y.-C. MAO, *Acta Phys. Chim. Sin.* , 2011, **27**, 1839-1846.
37. P. Xu, H. Shen, L. Yang, Y. Ding, B. Li, Y. Shao, Y. Mao and G. Li, *J. Mol. Model*, 2013, **19**, 551-558.
38. J. Wu, X. Zhen, H. Shen, G. Li and P. Ren, *J. Chem. Phys.*, 2011, **135**, 155104.
39. H. Shen, Y. Li, P. Ren, D. Zhang and G. Li, *J. Chem. Theory Comput.*, 2014, **10**, 731-750.
40. K. Katagiri, M. Hashizume, K. Ariga, T. Terashima and J. i. Kikuchi, *Chem. Eur. J.*, 2007, **13**, 5272-5281.
41. W. L. Jorgensen, D. S. Maxwell and J. Tirado-Rives, *J. Am. Chem. Soc.*, 1996, **118**, 11225-11236.
42. M. J. Schnieders and J. W. Ponder, *J. Chem. Theory Comput.*, 2007, **3**, 2083-2097.
43. S. L. Leung, Z. Zha, W. Teng, C. Cohn, Z. Dai and X. Wu, *Soft Matter*, 2012, **8**, 5756-5764.
44. Y. Jin, X. Yue, Q. Zhang, X. Wu, Z. Cao and Z. Dai, *Acta Biomater.*, 2012, **8**, 3372-3380.
45. Z. Cao, Y. Ma, X. Yue, S. Li, Z. Dai and J. Kikuchi, *Chem. Commun.*, 2010, **46**, 5265-5267.
46. S. K. Sahu, S. Maiti, A. Pramanik, S. K. Ghosh and P. Pramanik, *Carbohydr. Polym.*, 2012, **87**, 2593-2604.
47. Y. Ma, Z. Dai, Y. Gao, Z. Cao, Z. Zha, X. Yue and J.-I. Kikuchi, *Nanotoxicology*, 2011, **5**, 622-635.
48. T. Wang, F. Chai, Q. Fu, L. Zhang, H. Liu, L. Li, Y. Liao, Z. Su, C. Wang and B. Duan, *J Mater Chem*, 2011, **21**, 5299-5306.
49. C. A. Reddy, V. Somepalli, T. Golakoti, A. K. Kanugula, S. Karnewar, K. Rajendiran, N. Vasagiri, S. Prabhakar, P. Kuppusamy and S. Kotamraju, *PLOS ONE*, 2014, **9**, e89351.

View Article Online
DOI: 10.1039/C5TB01197C

A general and facile synthesis method was reported to fabricate TPP modified liposomal cerasomes as nanocarrier for mitochondria-targeted drug delivery.